PNAS RESEARCH ARTICLE | PLANT BIOLOGY

Chemical genetic screening identifies nalacin as an inhibitor of GH3 amido synthetase for auxin conjugation

Yinpeng Xie[a,b,c,1], Ying Zhu[a,b,1], Na Wang[a,b,1,2], Min Luo[a,b], Tsuyoshi Ota[d], Ruipan Guo[e,3], Ikuo Takahashi[d], Zongjun Yu[a,b], Yalikunjiang Aizezi[a,b], Linlin Zhang[a,b], Yan Yan[a,b], Yujie Zhang[d], Hongyu Bao[a,b], Yichuan Wang[a,b], Ziqiang Zhu[f], Ancheng C. Huang[a,b], Yunde Zhao[e], Tadao Asami[d], Hongda Huang[a,b,4], Hongwei Guo[a,b,4], and Kai Jiang[a,b,4]

Edited by Bonnie Bartel, Rice University, Houston, TX; received June 6, 2022; accepted November 1, 2022

Auxin inactivation is critical for plant growth and development. To develop plant growth regulators functioning in auxin inactivation pathway, we performed a phenotype-based chemical screen in Arabidopsis and identified a chemical, nalacin, that partially mimicked the effects of auxin. Genetic, pharmacological, and biochemical approaches demonstrated that nalacin exerts its auxin-like activities by inhibiting indole-3-acetic acid (IAA) conjugation that is mediated by Gretchen Hagen 3 (GH3) acyl acid amido synthetases. The crystal structure of Arabidopsis GH3.6 in complex with D4 (a derivative of nalacin) together with docking simulation analysis revealed the molecular basis of the inhibition of group II GH3 by nalacin. Sequence alignment analysis indicated broad bioactivities of nalacin and D4 as inhibitors of GH3s in vascular plants, which were confirmed, at least, in tomato and rice. In summary, our work identifies nalacin as a potent inhibitor of IAA conjugation mediated by group II GH3 that plays versatile roles in hormone-regulated plant development and has potential applications in both basic research and agriculture.

auxin conjugation | Gretchen Hagen 3 | chemical genetics | root development | plant growth regulator

Indole-3-acetic acid (IAA), the main natural auxin, regulates plant growth and development on the basis of its local concentration (1, 2). Thus, IAA homeostasis must be tightly controlled by coordination of its biosynthesis, transport, storage, and inactivation (3). Recent studies showed that IAA oxidation and conjugation are the two major routes for auxin inactivation (4). DIOXYGENASE FOR AUXIN OXIDATION (DAO), which belongs to the 2-oxoglutarate-dependent Fe(II) dioxygenase family, was first identified as an enzyme for auxin oxidation in rice (*Oryza sativa*) (5). Two DAO homologs, DAO1 and DAO2, have been identified in Arabidopsis, and their roles in auxin oxidation were characterized (6, 7). A *dao1* mutant with substantially decreased oxIAA levels showed no obvious changes in IAA levels but had an increase in IAA-Glu, indicating the importance of amino acid conjugation to the regulation of IAA homeostasis (6, 7). The Gretchen Hagen 3 (GH3) proteins are a family of acyl-acid-amido synthetases that conjugate amino acids to various substrates (8, 9). According to the sequence homology and substrate preference, nineteen GH3s in Arabidopsis can be categorized into three groups (10). Group II GH3, including GH3.1, GH3.2, GH3.3, GH3.4, GH3.5, GH3.6, GH3.9, and GH3.17, has been reported to mainly catalyze IAA conjugation to amino acids as a reversible storage form (9, 11). In addition to conjugating IAA, GH3.5 displays a wide preference for substrates, including salicylic acid (SA) (12). GH3.11 from group I prefers to catalyze conjugation of jasmonic acid (JA) to isoleucine (8, 13). GH3.12 and GH3.7 from group III accept isochorismate as the substrate to produce isochorismate-glutamate, a precursor that can be converted to SA (14, 15). However, due to the functional redundancy of group II GH3s, the studies on biological roles of GH3s that mediate IAA conjugation in planta still lag behind.

Chemical biology provides a powerful toolset of small molecules with which to explore biological processes (16). Small organic molecules can be applied to any plant tissue at appropriate concentrations at any stage of the plant life cycle and provide the advantage of avoiding complications arising from gene redundancy and lethal mutations (17). Although many chemical regulators have been developed and widely used for regulating auxin biosynthesis, transport, and signaling, the regulators of auxin catabolism pathway are still rare (18, 19). Adenosine-5'-[2-(1H-indol-3-yl)ethyl]phosphate (AIEP), a rationally designed inhibitor of GH3, displays potent inhibition on IAA conjugation in vitro (20), despite that its biological effects in broader plant species are yet to be defined. A recent study reported kakeimide (KKI) as a GH3 inhibitor, which has been applied to the study of the physiological roles of GH3s (11, 21).

Significance

Plants rely on the homeostasis of auxin to regulate plant growth and development, as well as to respond to various environmental cues. GH3-mediated auxin conjugation pathway is indispensable to this process. Here, we identified nalacin, an artificial small molecule that regulates root architecture and hypocotyl growth via inhibiting IAA-conjugating GH3s. Notably, the analyses of crystal structure and the docking simulation reveal the molecular basis of nalacin for preferred inhibition of group II GH3 and indicate its broad bioactivity in vascular plants. This work provides a well-defined inhibitor of GH3s as a chemical tool for the studies on the biological roles of GH3s in various plants and potential application as a plant growth regulator in agriculture.

The authors declare no competing interest.

This article is a PNAS Direct Submission.

[1]Y.X., Y.Z., and N.W. contributed equally to this work.

[2]Present address: Institutes of Physical Science and Information Technology, Anhui University, Hefei 230601, Anhui, China.

[3]Present address: The Cancer Hospital of the University of Chinese Academy of Sciences (Zhejiang Cancer Hospital), Institute of Basic Medicine and Cancer, Chinese Academy of Science, Hangzhou 310000, China.

[4]To whom correspondence may be addressed. Email: huanghd@sustech.edu.cn, guohw@sustech.edu.cn, or jiangk@sustech.edu.cn.

This article contains supporting information online at https://www.pnas.org/lookup/suppl/doi:10.1073/pnas.2209256119/-/DCSupplemental.

Published December 1, 2022.

Here, we performed a phenotype-based chemical screen for compounds regulating auxin catabolism in Arabidopsis and identified nalacin that displays auxin-like activities. Based on in vitro and in planta assays, we confirmed that nalacin exerts its auxin-like bioactivities by directly binding to several group II GH3 enzymes and inhibiting their catalysis of IAA conjugation. Crystal structural analysis together with docking simulation suggests the molecular basis for the activity of nalacin as an inhibitor across group II GH3 of Arabidopsis and indicates its broad bioactivity in other vascular plants, as demonstrated for tomato and rice. In summary, we report nalacin and its derivative D4 as inhibitors of GH3 enzymes that catalyze amido conjugation of IAA, and provide a chemical tool for the functional study of *GH3* genes in hormone-regulated plant development as well as potential agricultural application.

Results

Nalacin Is a Plant Growth Regulator with Auxin-Like Activities. To develop plant growth regulators (PGRs) that alter plant architecture, we performed a chemical screen (using a building block containing 11,800 chemicals from Life Chemicals) by observing the morphological changes in the roots of Arabidopsis wild-type Col-0 (Fig. 1*A*). We discovered that the compound *N*-[4-[[6-(1*H*-pyrazol-1-yl)-3-pyridazinyl]amino]phenyl]-3-(trifluoromethyl)benzamide (Fig. 1*B*) has versatile effects on the development of root architecture together with other effects on hypocotyl elongation and cotyledon epinasty (Fig. 1*C*), which are reminiscent of the effects of auxin. We designated the candidate compound as nalacin for its function as a non-auxin-scaffold-like auxin conjugation inhibitor, as indicated by the results detailed later in this article. Further physiological analyses showed that nalacin inhibited primary root growth and promoted adventitious root formation, lateral root number, and root hair elongation in a similar manner to IAA (Fig. 1 *D–F* and *SI Appendix*, Fig. S1). Consistent with these auxin-like activities, we found that nalacin triggered fluorescence signal changes in *DII-VENUS* and *DR5::GFP*, two marker lines for auxin response, in the same manner as IAA (Fig. 2 *A* and *B*), suggesting that nalacin plays a role in activating auxin signaling.

We also noticed additional and stronger effects of nalacin in promoting adventitious root formation and hypocotyl elongation in comparison with IAA (Fig. 1 *D*, *F*, and *G*). We found that nalacin triggered *DR5*-driven β-glucuronidase (GUS) signal in basal hypocotyl and lateral root primordium, which was not detected in the IAA-treated seedlings (*SI Appendix*, Fig. S2*A*). *GH3.3*, a marker gene for auxin rapid response, is rapidly upregulated by auxin treatment and then decreases due to negative feedback regulation (22). Notably, compared to IAA, nalacin produced a slower, longer-lasting induction of *GH3.3* expression in wild-type Col-0 and fluorescence signal in *DR5::GFP* line (Fig. 2*C* and *SI Appendix*, Fig. S2*B*). Together, these data indicate

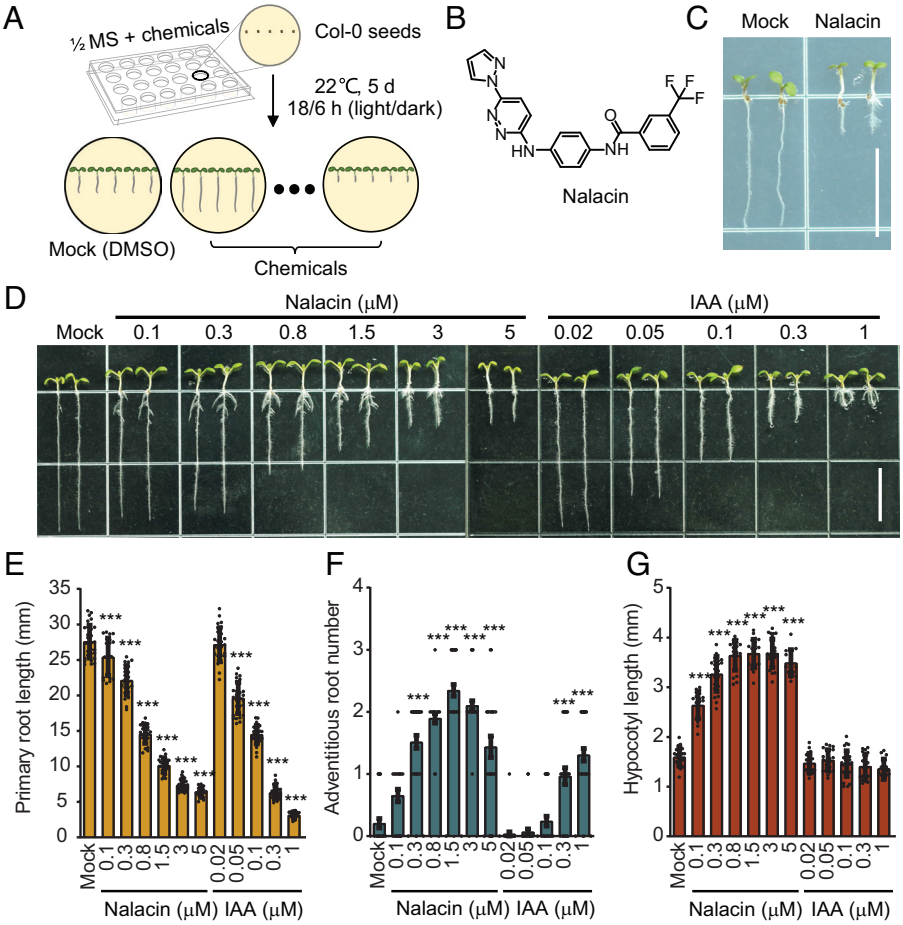

Fig. 1. Nalacin partially mimics IAA in inducing root phenotypes. (*A*) A schematic graph of chemical screening for plant growth regulator. (*B*) The chemical structure of nalacin. (*C*) 5-d-old Col-0 seedlings grown vertically on Murashige and Skoog (MS) medium containing 10 μM nalacin or dimethyl sulfoxide (DMSO) as the mock control. (Scale bar, 10 mm.) (*D*) 6-d-old Col-0 seedlings grown vertically on MS medium containing gradient concentrations of nalacin, IAA, or DMSO as the mock control. (Scale bar, 10 mm.) (*E–G*) Quantification of the primary root length, adventitious root number, and hypocotyl length of seedlings shown in (*D*). Values represent means and ±SD (n ≥ 15). Statistical significances were analyzed by two-way ANOVA along with Tukey's comparison test (***$P < 0.001$).

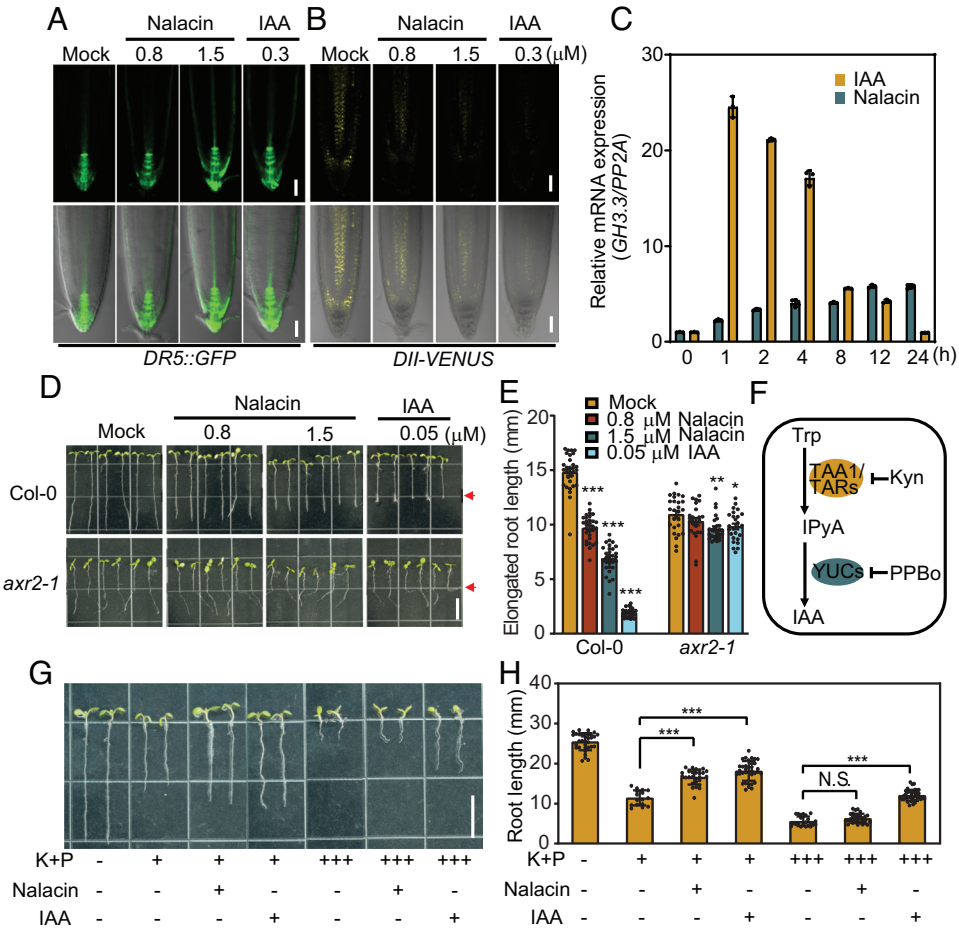

Fig. 2. Nalacin activates auxin signaling in IAA biosynthesis-dependent manner. (*A*) GFP fluorescence in the primary root of *DR5::GFP* reporter line. (Scale bar, 50 μm.) (*B*) YFP fluorescence in the primary root of *DII-VENUS* line. (Scale bar, 50 μm.) (*C*) Time-course expression of *GH3.3* in 6-d-old seedlings treated with 3 μM nalacin or 0.3 μM IAA in liquid MS medium. (*D*) 4-d-old seedlings were transferred to MS medium containing nalacin, IAA, or DMSO for 2 d. Red arrows indicate the initial transfer location of root. (Scale bar, 10 mm.) (*E*) Quantification of the primary root length of seedlings shown in (*D*). (*F*) A schematic diagram of Trp-dependent pathway for IAA biosynthesis. (*G*) 6-d-old Col-0 seedlings grown on MS medium containing combinatory treatment of 0.5 μM (+) or 10 μM (+++) Kyn and PPBo (K + P) together with nalacin (1.5 μM), IAA (0.02 μM), or DMSO. (Scale bar, 10 mm.) (*H*) Quantification of the root length shown in (*G*). Values represent means and ±SD (n ≥ 15). Statistical significances were analyzed by two-way ANOVA along with Tukey's comparison test (*$P < 0.05$, **$P < 0.01$, ***$P < 0.001$), N.S. indicates not significant.

that nalacin is a regulator of plant architecture that may act by activating auxin signaling in a spatiotemporal manner different from that of exogenous IAA.

Nalacin Exerts Bioactivities in an IPyA-Dependent Auxin Biosynthesis Pathway. To gain insights into nalacin's mode of action, we investigated its relationship with auxin via genetic and pharmacological analyses. *axr2-1* is a gain-of-function mutant line with a non-degradable IAA7 that disrupts an early step in auxin response (23, 24). Compared to Col-0, *axr2-1* displayed resistance to both IAA- and nalacin-induced inhibition of the primary root elongation (Fig. 2 *D* and *E*), suggesting that a functional auxin signaling pathway is required for their bioactivity. L-kynurenine (Kyn) and 4-phenoxyphenylboronic acid (PPBo) are two inhibitors of IAA biosynthesis that target the TAA1 and YUCs enzymes, respectively, to decrease endogenous IAA levels (Fig. 2*F*) (25, 26). Combination treatment with Kyn and PPBo (K + P) resulted in a short primary root (Fig. 2 *G* and *H*) due to their pharmacological role in decreasing local IAA level. Treatment with either nalacin or IAA partially restored the primary root growth that was suppressed by 0.5 μM K + P (Fig. 2 *G* and *H*). However, when suppressed by a higher concentration of K + P (10 μM), the primary root growth could be partially restored by treatment with IAA but not nalacin (Fig. 2 *G* and *H*), suggesting that nalacin cannot substitute for endogenous IAA in planta. To further test whether nalacin is an auxin mimic, we performed a yeast three-hybrid assay and found that IAA but not nalacin promoted the interaction of INDOLE-3-ACETIC ACID INDUCIBLE5 (IAA5) with auxin receptors TRANSPORT INHIBITOR RESPONSE1 (TIR1) and AUXIN SIGNALING F-BOX PROTEIN2 (AFB2), respectively (*SI Appendix*, Fig. S2*C*). Collectively, these results suggest that nalacin is not an auxin mimic per se and that its auxin-like activity is dependent on endogenous IAA biosynthesis, possibly via its impact on IAA homeostasis.

Nalacin Increases Endogenous IAA Level via Inhibition of IAA Conjugation. To validate the effects of nalacin on IAA homeostasis, we quantified the levels of IAA, its biosynthesis precursors (Trp and IPyA), and major inactivated metabolites in Col-0, including oxIAA and amino-acid-conjugated IAAs (IAA-Glu and IAA-Asp) whose formation is catalyzed by DAOs and GH3s, respectively (6, 7, 9). Compared to the mock treatment, the Trp and IPyA contents were not altered after nalacin treatment (Fig. 3 *A* and *B*), while nalacin increased IAA levels and decreased the levels of IAA-Asp and IAA-Glu without changing the levels of oxIAA (Fig. 3 *C*–*F*). These results strongly imply that nalacin exerts

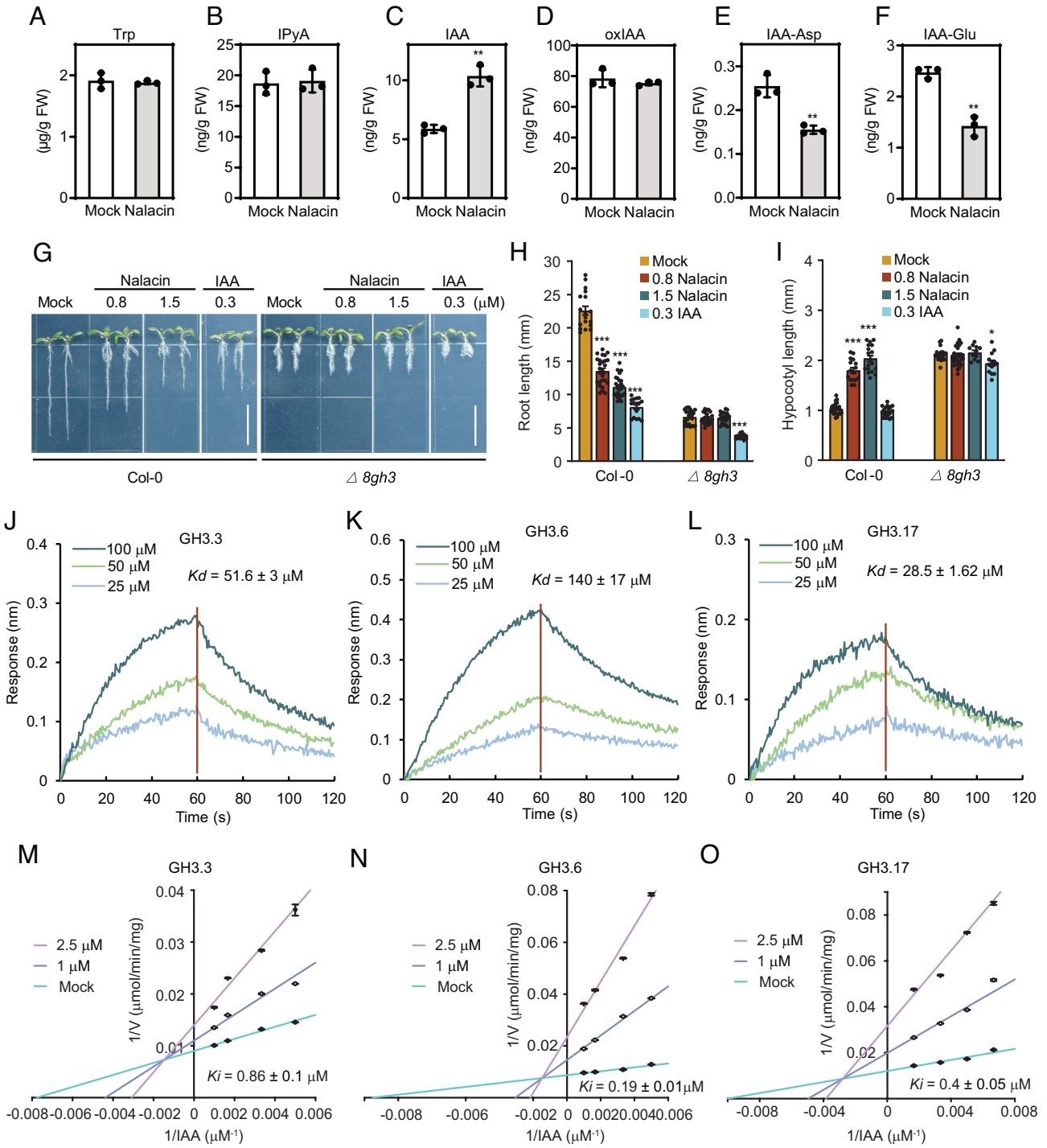

Fig. 3. Nalacin inhibits GH3-mediated IAA conjugation in vivo and in vitro. (*A–F*) Determination of IAA, IAA biosynthetic precursors (Trp and IPyA), and major metabolic products (IAA-Glu, IAA-Asp, and oxIAA) under 3 μM nalacin or DMSO treatment in Col-0. 6-d-old seedlings of Col-0 were transferred onto the filter papers which wetted by liquid MS medium supplemented with 3 μM nalacin or DMSO as the mock control for 2 h. (*G*) Representative seedlings of 6-d-old Col-0 and Δ*8gh3* grown on MS medium containing nalacin, IAA, or DMSO as the mock control. (*H* and *I*) Quantification of the root length and hypocotyl length shown in (*G*). Values represent means and ±SD (n ≥ 15). (*J–L*) BLI assay on the kinetic interactions of nalacin with GH3.3, GH3.6, and GH3.17. Biotinylated GH3 proteins were loaded on SSA sensors followed by exposure to gradient concentrations of nalacin (3.125–25 μM). (*M–O*) Kinetic analysis of the inhibition of nalacin on GH3.3, GH3.6, and GH3.17. The production of IAA-Asp (for GH3.3, GH3.6) and IAA-Glu (GH3.17) were detected by UPLC-MS. Double-reciprocal plots of initial velocities (Lineweaver–Burk plots) showing mixed-type inhibition. Values represent means and ±SD (n ≥ 3). Statistical significances were analyzed by two-way ANOVA along with Tukey's comparison test for (*H* and *I*) and Student's *t* test for (*A–F*) (*$P < 0.05$, **$P < 0.01$, ***$P < 0.001$).

its auxin-like activities via inhibiting the inactivation of IAA by amino acid conjugation, which leads to higher levels of active IAA.

As stated above, nineteen GH3 can be divided into three phylogenetic groups (*SI Appendix*, Fig. S3*A*), among which the group II GH3s are responsible for amino acid conjugation of IAA (9). We found that Δ*8gh3* (a mutant with loss of function of all eight group II GH3s) was resistant to nalacin treatment, while still being responsive to exogenous IAA treatment (Fig. 3 *G–I*). Moreover, the endogenous levels of IAA and metabolites showed no response to nalacin treatment in the Δ*8gh3* (*SI Appendix*, Fig. S4 *A–F*). Auxin shapes gene expression to regulate plant growth and development (27–29). To investigate the gene expression pattern of

Col-0 and Δ*8gh3* in response to nalacin treatment, we performed a transcriptome profiling. Compared to the mock treatment, nalacin triggered expression changes in 169 genes in Col-0 (*SI Appendix*, Fig. S5*A* and Table S1). Gene ontology (GO) analysis of biological processes showed that these differentially expressed genes (DEGs) can be enriched for auxin response (*IAA1/2/19/30* and *GH3.1/2/3/5/6*) and the formation of lateral root and callus (*LBD16/18/29*) (*SI Appendix*, Fig. S5 *B* and *C* and Table S1), which can be highly induced by IAA treatment as well (27–29). In contrast, nalacin only induced 13 DEGs in Δ*8gh3* (*SI Appendix*, Fig. S5*D* and Table S2), which are not enriched for any biological or signal processes by GO analysis. In addition, none of DEGs were the typical genes related to auxin (*SI Appendix*, Fig. S5*D* and Table S2). These results collectively indicate that nalacin influences IAA homeostasis via targeting group II GH3s.

Nalacin Directly Interacts with GH3s and Suppresses Their Enzymatic Activity on Amino Acid Conjugation of IAA. To test whether group II GH3 enzymes are the direct targets of nalacin, we selected GH3.3, GH3.6, and GH3.17 as representatives for each subgroup of group II GH3 based on phylogenetic analysis (*SI Appendix*, Fig. S3*B*) and produced recombinant proteins of these three GH3 proteins via *Escherichia coli*. We performed a biolayer interferometry (BLI) assay and found that nalacin displayed slow association and dissociation kinetics for GH3.3, GH3.6, and GH3.17 (K_d values of 51.6 μM, 140 μM, and 28.5 μM, respectively) (Fig. 3 *J*–*L*), indicating a direct binding of nalacin to these GH3s. We further performed in vitro enzyme kinetic analyses and found that nalacin inhibited the amino acid conjugation of IAA catalyzed by GH3.3, GH3.6, and GH3.17 at submicromolar concentrations (K_i values were 0.86 μM, 0.19 μM, and 0.4 μM, respectively) (Fig. 3 *M*–*O*). The double-reciprocal plots of initial velocities (Lineweaver–Burk plots) indicate that nalacin is a competitive and uncompetitive mixed-type inhibitor, which could bind to both free enzyme and substrate-bound enzyme. Compared to AIEP, a competitive GH3 inhibitor with IAA scaffold (12, 20), nalacin functions as a non-auxin-scaffold-like auxin conjugation inhibitor with a different inhibitory mode of action. It is worth to note that GH3.5 displays dual function in amino acid conjugation of both IAA and SA (12, 30). Compared with the mock treatment, the endogenous concentration of SA in Col-0 was not altered upon nalacin treatment (*SI Appendix*, Fig. S6*A*). This result indicates that GH3.5-mediated SA conjugation is not affected by nalacin, which could be attributed to lower efficiency of GH3.5 in catalyzing SA (*K*m = 1171 μM) than that of IAA (*K*m = 45 μM) (30) or other reasons yet to be determined.

Arabidopsis GH3 proteins share the same Ping-Pong reaction mechanism for catalyzing the conjugation of versatile substrates, including IAA, JA, and salicylic acid (12, 31, 32). To investigate whether nalacin targets GH3s in other groups, we selected GH3.11 and GH3.12 as representative members of group I and group III GH3, respectively. We observed no inhibitory effect of nalacin on GH3.12 for catalyzing its substrate 4-HBA into 4-HBA-Glu via in vitro assay (*SI Appendix*, Fig. S6 *C*–*E*) (33). GH3.12 is also reported to catalyze the conjugation of glutamate to isochorismate and produce isochorismate-9-glutamate, which spontaneously converts into SA in planta (15). Consistent with our in vitro result, we observed no significant change of SA levels between nalacin-treated seedlings and the mock-treated ones in Col-0 and Δ*8gh3* (*SI Appendix*, Fig. S6 *A* and *B*), indicating nalacin has no influence on GH3.12. In contrast, we found that nalacin suppressed the Ile conjugation of JA catalyzed by GH3.11 with a mixed-type inhibition (*SI Appendix*, Fig. S7*A*). We also observed decrease in endogenous levels of JA-Ile in nalacin-treated Col-0 and Δ*8gh3* (*SI Appendix*, Fig. S7 *B* and *C*). These results indicate that nalacin inhibits GH3.11 both in vitro and in planta. However, nalacin-induced phenotype changes in root and hypocotyl are not attributed to nalacin's inhibition on GH3.11 as no significant difference was observed between Col-0 and *jar1-1*, a *gh3.11* mutant, in terms of these phenotypes, and their responses to nalacin were quite similar (*SI Appendix*, Fig. S7 *D*–*F*). Thus, we focus on investigating nalacin's mode of actions on group II GH3 enzymes that mediate auxin homeostasis although it might affect other JA-involved processes not observed in current assays.

Structure–Activity Relationship Analysis of Nalacin Identifies a Bioactive Derivative. During the nalacin synthesis process, we obtained four intermediate chemicals that partially share common moieties with nalacin. We designated them D1–D4 and tested their bioactivities (Fig. 4). We observed no phenotypic changes in seedlings treated by D1 or D2. D3 displayed weak bioactivities in promoting adventitious root and inhibiting primary root growth at relatively high concentration level (1.5 μM) (Fig. 4 *B*–*D*). D4 showed an effect similar to nalacin in promoting adventitious root number and hypocotyl elongation, except that its inhibition of primary root growth was weaker (Fig. 4 *B*–*E*). In support of the physiological observations, we observed that D4 inhibited IAA-Asp production catalyzed by GH3.6 with a K_i of 0.3 μM (Fig. 4*F*). These results indicate that the *N*-(4-aminophenyl)-3-(trifluoromethyl)benzamide moiety represented by D3, rather than those represented by D1 or D2, is the basic structure for the bioactivities. Introducing either pyrazol-1-yl-pyrizadine or chloropyrizadine moieties into D3, which produces nalacin and D4, respectively, dramatically increased the bioactivity. These structure–activity relationship studies identify a GH3 inhibitor D4 and provide information for further chemical modifications on nalacin.

Structural Analysis of the GH3.6-AMP-D4 Complex. To investigate the molecular basis of nalacin and D4 inhibition of group II GH3 proteins, we tried to crystallize the Arabidopsis GH3.6 protein in complex with nalacin or D4 alone or in combination with other substrates or products, including adenosine triphosphate (ATP), adenosine-5'-(γ-thio)-triphosphate (ATPγS), adenosine monophosphate (AMP), and Mg^{2+}. We successfully crystallized the GH3.6–AMP–D4 complex and solved its crystal structure to 2.40 Å (*SI Appendix*, Table S3). The structure of this complex adopts a closed active site conformation (Fig. 5*A*) (12, 31), and the overall fold of GH3.6 resembles the fold of other GH3-family proteins, with a large N-terminal α/β fold domain (residues 1–446 in GH3.6), a small C-terminal domain (residues 460–612), and a hinge loop (residues 447–459) connecting them (Fig. 5 *A* and *B*) (12). Structural comparisons revealed that the conformation of the GH3.6 C-terminal domain is indeed highly similar to its counterparts in the closed-form structures of the Arabidopsis GH3.5 (12), GH3.12 (14, 31, 34), and GH3.11 (31), with small displacement observed as compared to GH3.11 (*SI Appendix*, Fig. S8 *A*–*C*). As expected, the conformation of the GH3.6 C-terminal domain is significantly different from that in the open-form structures of GH3.12 (31) and GH3.15 (35, 36) with a 180°-rotation, and from that in the complex-form structure of GH3.11 (37) with big movement and rotation (*SI Appendix*, Fig. S8 *D*–*F*). These observations further confirmed the conformational flexibility in the C-terminal domain of GH3 enzymes that may correlate with different catalysis steps.

In the GH3.6–AMP–D4 complex structure, AMP is bound in the nucleotide-binding site of GH3.6, which is conserved in

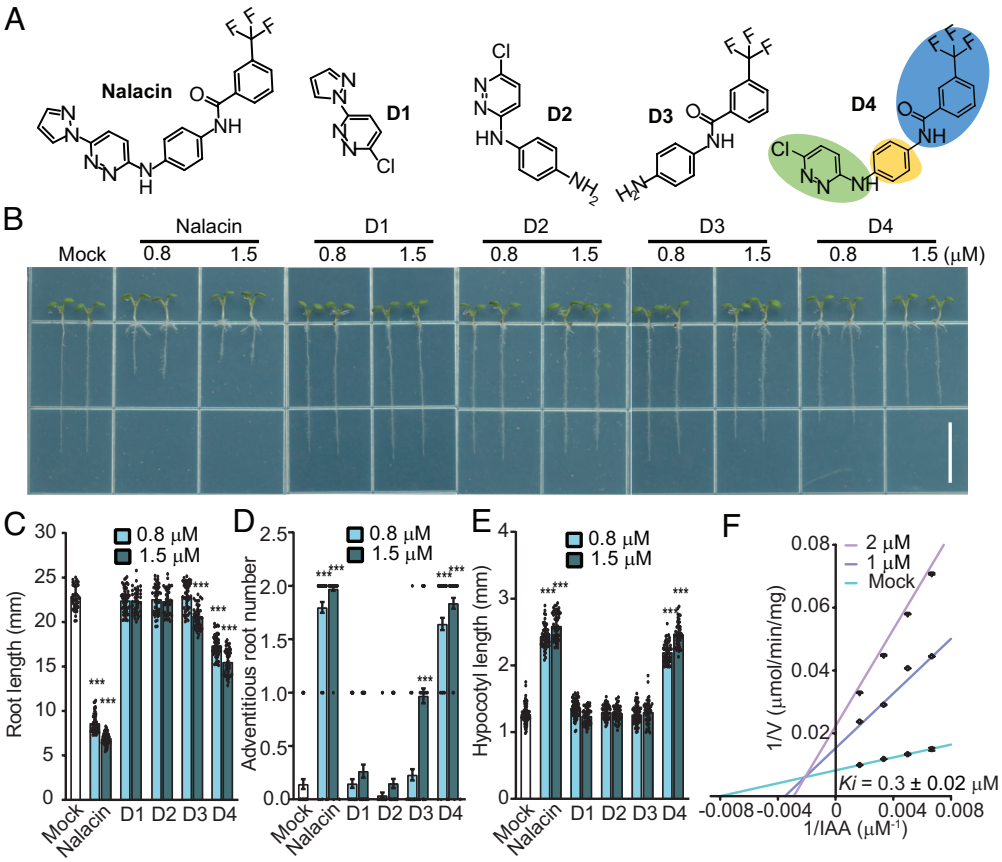

Fig. 4. Structure–activity relationship analysis of nalacin. (*A*) Structures of nalacin and its derivatives D1, D2, D3, and D4. The structure of D4 is subdivided into three parts, including trifluoromethylbenzamide portion (part I), phenyl portion (part II), and aminochloropyridazine portion (part III) highlighted in blue, yellow, and green colors, respectively. (*B*) Representative Col-0 seedlings vertically grown on MS medium containing chemicals for 6 d. (Scale bar, 10 mm.) (*C*–*E*) Quantification of the primary root length, adventitious root number, and hypocotyl length of the seedlings treated by chemicals or DMSO as the mock control. Values represent means and ±SD (n ≥ 15). (*F*) Kinetic analysis of the inhibition of D4 on GH3.6. The production of IAA-Asp was detected by UPLC-MS. Values represent means and ±SD (n ≥ 3). Statistical significance was analyzed by two-way ANOVA along with Tukey's comparison test (***$P < 0.001$). Data in (*B*–*F*) were derived from experiments that were performed three times with similar results, and representative data from one replicate were shown.

other GH3s (12, 31), indicative of their universal enzymatic mechanism (Fig. 5*C*). D4 is buried in a relatively hydrophobic channel that is also the acyl acid-binding pocket of the GH3-family proteins (12, 31), and has extensive interactions with GH3.6 and AMP (Fig. 5 *A*, *B*, and *D* and *SI Appendix*, Fig. S8*G*). For analysis, the structure of D4 can be subdivided into a trifluoromethylbenzamide portion (I), a phenyl portion (II), and an aminochloropyridazine portion (III) (Fig. 4*A*). The interactions within part I are as follows (Fig. 5 *B* and *D*): the trifluoromethyl group establishes van der Waals contacts (distance ≤ 4.0 Å) and an F···H-P hydrogen bond with the phosphate group of AMP, with the latter implying that the phosphate group of AMP is protonated; the trifluoromethyl group forms contacts with Ala339, Ser340, and S341 in the β8–turn–β9 motif; the phenyl ring forms CH-π stacking with Met337 and Ala339 on one side and Ile312 on the opposite side, and also contacts Leu175 and the adenine moiety of AMP; and the carbonyl group is hydrogen-bonded to Tyr134. Within part II (Fig. 5*D*), the phenyl group establishes T-shaped π-π stacking with Tyr134, and one edge of the phenyl group forms OH-π and CH-π attractions with Tyr179 and Val231, respectively. Lastly, within part III (Fig. 5*D*), the amine group and one nitrogen atom of the pyridazine group are each hydrogen-bonded to Tyr195; the pyridazine group establishes Y-shaped π-π stacking with Tyr134 and Phe184 and also contacts Tyr178 and Thr193; and the chloride atom forms some contacts with Tyr178.

Structural Analysis of Nalacin's Binding Mode to GH3s in Arabidopsis. To analyze the molecular modes of action of nalacin, we performed a molecular docking simulation based on the structure of the GH3.6–AMP–D4 complex. As expected, we redocked D4 to GH3.6 in almost the same pose as observed in the crystal structure (*SI Appendix*, Fig. S9) and with a reasonable docking scoring (*S* –8.0900), suggesting the reliability of our docking process. Nalacin was docked to GH3.6 and superposed well with D4 except for its additional pyrazole moiety (Fig. 5*E*), which introduces a CH-π interaction with Thr193 and may contribute to its better affinity for GH3.6 (S –8.6907) and greater bioactivity as compared to D4 (Fig. 4 *B*–*E*). D1, D2, and D3 have interaction poses that clearly differ from those of nalacin and D4, according to the docking analysis, and have low affinities for GH3.6, as represented by poor docking scorings (S –5.4018, –5.8495, and –6.5732, respectively) (*SI Appendix*, Fig. S9), in line with their bioactivities (Fig. 4 *B*–*E*). In view of the fact that ATP shares similar binding sites with AMP (12, 31) and nalacin contacts only the alpha phosphate group of AMP (Fig. 5*D*), nalacin may also bind to GH3.6 in complex with ATP. We performed a BLI assay and confirmed that nalacin displayed fast association and dissociation kinetics with reasonable affinities for GH3.6 in the presence of AMP or ATP (K_d values of 49 and 26 μM, respectively) (Fig. 5*F*). These biochemical results, together with the structural information, suggest that nalacin can inhibit AMP- or ATP-bound GH3s.

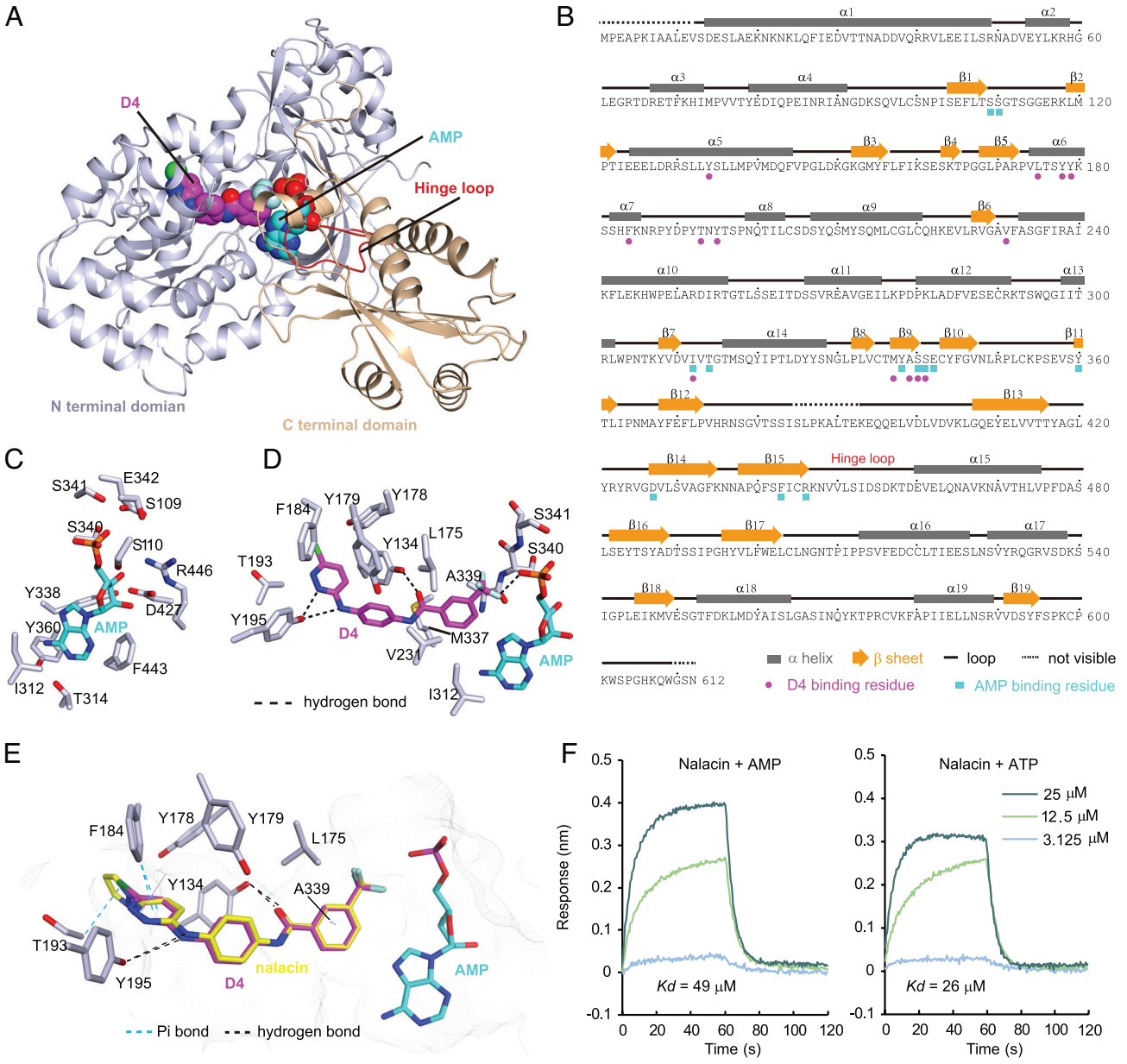

Fig. 5. Structural analysis of the GH3.6-AMP-D4/nalacin complex. (*A*) Overall structure of the GH3.6-AMP-D4 complex, adopting a closed active site conformation. The N- and C-terminal domains and the hinge loop connecting them are highlighted. The bound AMP and D4 molecules are shown in sphere mode. (*B*) The sequence and secondary structures of GH3.6 derived from the complex structure. The residues interacting with D4 and AMP are highlighted with magenta circles and cyan squares, respectively. (*C*) The conserved AMP-binding site of GH3.6. (*D*) An enlarged view showing the detailed interactions of D4 with GH3.6 and AMP. (*E*) A site view of molecular docked nalacin (in yellow color) superposed with D4 (in purple color) from the crystal structure. (*F*) BLI assay on the kinetic interactions of nalacin with GH3.6 in the presence of AMP or ATP. Biotinylated GH3 proteins were loaded on SSA sensors followed by exposure to gradient concentrations of nalacin (3.125–25 μM) and fixed concentration of AMP (100 μM) or ATP (100 μM). Data in (*F*) were derived from experiments that were performed two times with similar results, and representative data from one replicate were shown.

Whether nalacin is a selective inhibitor for a unique group of GH3s or a pan-inhibitor for all GH3s remained unknown. We analyzed the binding pockets of all GH3s by sequence alignment and comparing their three-dimensional structures obtained from the Protein Data Bank (PDB), AlphaFold (38), and our de novo homology modeling results (*SI Appendix*, Fig. S10). We found that the overall folds are generally conserved in each GH3 group (*SI Appendix*, Fig. S10*A*). As expected, all GH3s have a set of conserved residues for binding ATP and AMP (*SI Appendix*, Fig. S10 *B* and *D*), which are the common substrate and product for catalysis by GH3s. In contrast, the residues constituting the pocket that binds nalacin/D4 are highly conserved in group II but not in groups I or III GH3s (*SI Appendix*, Fig. S10 *C* and *D*), suggesting a preference of nalacin/D4 for group II GH3s. It is noteworthy that 13 residues of GH3.6 for interacting with nalacin/D4 are not all conserved in GH3.4 and GH3.9 (*SI Appendix*, Fig. S10*D*). Two residues Tyr134 and Thr193 in GH3.6 that form multiple interactions with nalacin/D4 were replaced by Gly and Ser, respectively, in GH3.4, while Tyr195 and Ile312 in GH3.6 were replaced by Leu and Val, respectively, in GH3.9 (*SI Appendix*, Fig. S10*D*), possibly leading to decreases in the binding affinities of nalacin/D4. In addition, we also noticed that GH3.10 and GH3.11 from group I, and GH3.7, GH3.12, and GH3.19 from group III possess several nalacin/D4-interacting residues (although not as many as in group II GH3s) (*SI Appendix*, Fig. S10*D*). These results and our in vitro and in vivo assays for the inhibitory effect

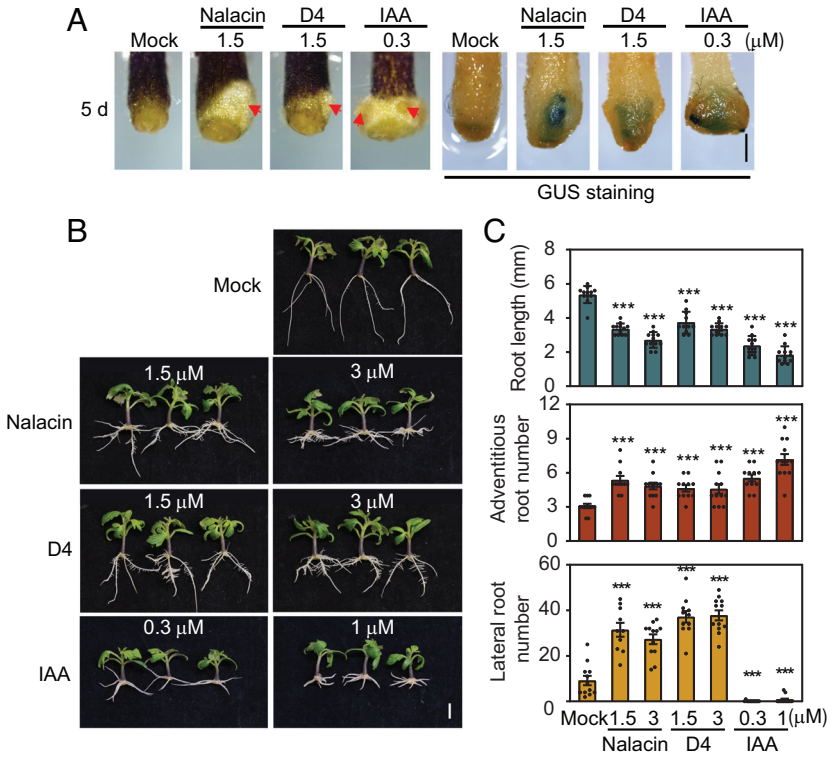

Fig. 6. Nalacin and D4 promote adventitious root development in tomato. (*A*) 7-d-old *DR5::GUS* seedlings of tomato had their roots removed and were transferred to MS medium containing nalacin, D4, IAA, or DMSO followed by additional cultivation for 5 d. Red arrows indicate the stem–root emergence in the base of the cuttings treated by nalacin, D4, or IAA. GUS staining of cut hypocotyls was performed on day 5 (cutting edge) after transferring. (Scale bar, 1 mm.) (*B*) Tomato cutting propagation assay. 7-d-old tomato seedlings were detached with root and transferred to MS medium containing nalacin, D4, IAA, or DMSO followed by additional cultivation for 10 d. (Scale bar, 1 cm.) (*C*) Quantification of the root length, adventitious root number, and lateral root number shown in (*B*). Statistical significance was analyzed by two-way ANOVA along with Tukey's comparison test (***$P < 0.001$). Data in (*A*–*C*) were derived from experiments that were performed two times with similar results, and representative data from one replicate were shown.

of nalacin on GH3.11 and GH3.12 (*SI Appendix*, Figs. S6 and S7) indicate that nalacin could bind to and inhibit other GH3s with a different manner from that of group II GH3 members. In spite of those possibilities, our structural analyses together with biochemical and biological studies strongly suggest that nalacin and D4 exert their auxin-like bioactivities via preferably targeting group II GH3.

To further obtain a structural insight into the inhibitory mode of nalacin substrate binding of GH3s, we performed molecular docking simulation of IAA, SA, and JA to GH3.6, GH3.5, and GH3.11, respectively (*SI Appendix*, Fig. S11 *A*–*F*), and analyzed the binding sites of these substrates relative to that of nalacin. We found that trifluoromethyl phenyl group of nalacin occupies the binding sites of IAA and JA in GH3.6 and GH3.11, respectively (*SI Appendix*, Fig. S11 *A*–*D*), suggesting nalacin's competitive inhibition on the substrate acceptance of GH3.6 and GH3.11 at the first step of Ping-Pong reaction. In contrast, the predicted SA-binding site in GH3.5 is away from that of nalacin (*SI Appendix*, Fig. S11 *E* and *F*), indicating that nalacin could not influence on SA-binding of GH3.5. Compared to AIEP, another GH3 inhibitor (12, 20), nalacin, occupies a broader space in the pocket of GH3 and possesses a pyrazol-1-yl-pyrizadine moiety that faces away from the enzymatic reaction center (*SI Appendix*, Fig. S11 *G* and *H*).

Nalacin Displays Productive Potential to Inhibit IAA-Conjugating GH3s in a Broad Range of Plant Species. Previous studies indicated that GH3 proteins were conserved in the plant kingdom (10). We performed BLAST analysis and alignment of the homologs of Arabidopsis GH3.6, using them as representatives of group II GH3s from lower plants to higher plants, including moss, liverworts, fern, monocots, and eudicots (*SI Appendix*, Fig. S12 *A* and *B*). We found that the residues that consist of the pocket and the nalacin- and D4-interacting residues are highly conserved in vascular plant species, implying that nalacin and D4 should also have bioactivity in other higher plant species. To validate this hypothesis, we performed a tomato cutting propagation assay, in which auxin plays a pivotal role (39). We found that nalacin, D4, and IAA induce stem–root emergence and *DR5*-driven GUS signals are observed at the base of cuttings (Fig. 6*A* and *SI Appendix*, Fig. S13 *A*–*C*). After long-time cultivation, nalacin and D4, but not IAA, triggered the initiation of lateral roots in adventitious roots (Fig. 6 *B* and *C*), indicating a potential role of auxin conjugation in lateral root development. Moreover, nalacin and D4 inhibited the root growth of rice seedlings (*SI Appendix*, Fig. S14) similarly to IAA (40). Taken together, the above results confirm that nalacin and its derivative D4 can inhibit group II GH3 and thus IAA conjugation, and have broad activities in various plant species.

Discussion

By a phenotype-based chemical screening, we identified nalacin, an artificial small molecule, that regulates root architecture in a similar manner to IAA (Figs. 1 and 2 *A*–*C* and *SI Appendix*, Fig. S1). We found that nalacin is not an auxin mimic (*SI Appendix*, Fig. S2*C*) and exerts its biological activities in an auxin biosynthesis-dependent manner (Fig. 2 *G* and *H*). Further studies confirmed that nalacin can directly bind to several group II GH3s (Fig. 3 *J*–*L*) and inhibit GH3-mediated conjugation of Glu or Asp to IAA (Fig. 3 *M*–*O*), leading to an increase in endogenous

IAA levels in planta (Fig. 3*C*). In addition, Δ*8gh3* showed resistance to nalacin treatment in both phenotypic changes and perturbation of endogenous IAA levels (Fig. 3 *G–I* and *SI Appendix*, Fig. S4*C*). These results together with transcriptome analysis (*SI Appendix*, Fig. S5 *A–D* and Tables S1 and S2) demonstrate that nalacin can inhibit group II GH3s and overcome their redundant roles in catalyzing IAA conjugation. Compared to Δ*8gh3* with defects in whole development stage, nalacin is expected to be temporally applied to dissect the biological roles of GH3s at any time point in the whole lifespan of plants. It is noteworthy that nalacin can also suppress JA-Ile production catalyzed by GH3.11, a group I GH3 member (*SI Appendix*, Fig. S7 *A–C*). In contrast, nalacin showed no inhibitory effect on GH3.12, a group III GH3 member (*SI Appendix*, Fig. S6 *C–E*). As the substrates of many GH3s are yet to be determined, thus, in comparison with one-at-a-time in vitro tests, a future metabolome analysis could give a comprehensive understanding of nalacin-triggered metabolite changes and the possible targets of nalacin. Nevertheless, our current results corroboratively demonstrate that nalacin and D4 are effective inhibitors of IAA-conjugating GH3s that can be applied to regulate auxin homeostasis.

Due to the feedback regulation of IAA by IAA-induced *GH3* transcript levels and subsequent inactivation by GH3-mediated conjugation, exogenous IAA treatment exerts bioactivity under strict regulation of GH3s upon their spatial-temporal expression pattern (41–47). Exogenous IAA treatment caused a rapid increase followed by a rapid decrease in *GH3.3* expression (Fig. 2*C*). In contrast, nalacin can trigger the accumulation of auxin and exert its auxin-like bioactivity without being strictly gated by GH3s and cause a mild, long-lasting increase in auxin signal (Fig. 2*C* and *SI Appendix*, Fig. S2*B*). We observed GUS signal accumulation in hypocotyl and hypocotyl–root junction in seedlings treated with nalacin rather than IAA (*SI Appendix*, Fig. S2*A*), which correlates with the stronger physiological effects of nalacin in promoting adventitious root formation and hypocotyl elongation (Fig. 1 *D*, *F*, and *G*). Thus, nalacin displays different morphological effects from IAA in a tissue-specific manner of GH3s. What's more, the fact that nalacin is an effective inhibitor that can nicely overcome gene redundancy provides a strategy for spatiotemporal regulation of GH3 enzyme, which can be used for both scientific research and agricultural application in non-model plants, such as root regeneration as demonstrated in this work.

In addition to nalacin, we also developed its derivative D4 and succeeded in resolving a complex structure of GH3.6 and D4 (Fig. 5 *A–D*). Based on the information from crystal structure and docking simulation, we found that nalacin- and D4-interacting residues are highly conserved in group II GH3s in Arabidopsis and various vascular plants (*SI Appendix*, Figs. S10*D* and S12), indicating their general bioactivities via targeting group II GH3s and thus perturbing IAA levels across the plant species. In support of that, we have confirmed that nalacin and D4 display auxin-like activities, at least, in Arabidopsis, tomato, and rice (Figs. 1 and 6 and *SI Appendix*, Figs. S13 and 14). In addition to the common bioactivities between nalacin and D4 (Fig. 4 *B*, *D*, and *E*), we also noticed their different effectiveness in suppressing the primary root growth (Fig. 4 *B* and *C*), which correlates with their inhibitory effects on GH3.6 (Figs. 3*N* and 4*F*), a key player in primary root growth. These results suggest a potential for developing selective GH3 inhibitors based on the scaffold of nalacin.

GH3-mediated IAA conjugation utilizes a "Bi Uni Uni Bi Ping-Pong" reaction that includes two successive steps (32). Our crystal structure and docking simulation results provide a structural basis for nalacin's binding and inhibitory mechanism in the view of the Ping-Pong reaction (Fig. 5 *A–E* and *SI Appendix*, Fig. S10). Nalacin occupies the binding sites of IAA and JA in the pockets of GH3.6 and GH3.11, respectively, but not the binding site of SA in the pocket of GH3.5 (*SI Appendix*, Fig. S11), suggesting nalacin's competitive inhibition on the first step of Ping-Pong reaction. In support of that, we observed inhibitory effects of nalacin on the catalysis of IAA and JA in both in vitro enzymatic assays (Fig. 3*N* and *SI Appendix*, Fig. S7*A*) and in planta assays (Fig. 3 *E* and *F* and *SI Appendix*, Fig. S7 *B* and *C*). In view of the complexity of the Ping-Pong reaction and nalacin's mixed-type inhibition on GH3s, it remains the possibility that nalacin could also inhibit GH3s with additional mode of actions yet to be further determined.

AIEP, an intermediate of the IAA conjugation reaction, displays competitive effect against both ATP and IAA binding to GH3 (20), while the biological activity of AIEP in planta has not determined yet. Recently, KKI was reported to be a selective inhibitor of group II GH3s that catalyze IAA conjugation (21). Kinetic analysis revealed that KKI binds to GH3–ATP to form a GH3–ATP–KKI complex and competitively inhibits the binding of IAA without influencing on ATP binding (21). Compared to AIEP and KKI, nalacin occupies the binding site of GH3s for acyl acid substrate and inner-side of the pocket but not the site for ATP binding (*SI Appendix*, Fig. S11), and displays a mixed-type inhibition on GH3s (Fig. 3 *M–O* and *SI Appendix*, Fig. S7*A*). Despite the difference in their inhibitory modes on GH3s, nalacin and KKI can trigger the common phenotypic changes in Arabidopsis Col-0, including short primary root, long hypocotyl, and increase in the numbers of lateral and adventitious roots, phenocopying Δ*8gh3*. These results suggest the effectiveness of nalacin and KKI as inhibitors of group II GH3s that mediate auxin homeostasis. It is interesting that both nalacin and KKI have a common benzamide portion, which introduces many interactions with the residues in GH3 pocket observed in our crystal structure (Fig. 5 *D* and *E*) and could be informative for further modifications on these two chemicals. Compared with KKI that only targets group II GH3s, nalacin can also inhibit GH3.11 with a different binding mode from that observed in GH3.6 (*SI Appendix*, Fig. S11 *A–D*), suggesting a need and also a potential to improve the selectivity of nalacin for distinct GH3 families via chemical modification. It is noteworthy that the inner-side pocket occupied by the pyrazol-1-yl-pyrizadine moiety of nalacin is distal to the enzyme reaction center (*SI Appendix*, Fig. S11), providing a potential avenue for genetic engineering of GH3s. The engineered GH3 variants would be expected to tolerate nalacin binding without impairing the original enzyme activity. In view of the auxin-like herbicidal effects of nalacin at high concentrations, the combinations of nalacin and the nalacin-tolerant GH3 variants may provide tool kits for the design of herbicide-tolerant crops or other deliberate regulatory changes.

Materials and Methods

Plant Materials. Unless otherwise indicated, all Arabidopsis mutants and transgenic lines employed in this study are in the Col-0 background. The Δ*8gh3* octuple mutant has been previously reported in the literature (41). The homozygous lines were identified by phenotype and genotype screening. Detailed descriptions of plant materials and growth conditions, treatments, and experimental methods are described in *SI Appendix, SI Materials and Methods*. Small molecule library and screen information, root hair length measurement and fluorescence observation, GUS staining, measurement of IPyA, IAA and IAA catabolites, enzymatic activity assay and kinetic analysis, BLI analysis, transcriptome sequencing and data analysis, crystallization and data collection, molecular docking simulation, homology modeling, and chemical preparation were carried out according to protocols described in *SI Appendix, SI Materials and Methods*.

Data, Materials, and Software Availability. Atomic coordinates and structure factors for the reported crystal structure have been deposited in the PDB under accession numbers 7VKA (the AtGH3.6-AMP-D4 complex). Sequencing data of mRNA are available at the NCBI database with the accession number PRJNA875587. All study data are included in the article and/or *SI Appendix*.

ACKNOWLEDGMENTS. We thank Dr. Yang Zhao (Shanghai Center for Plant Stress Biology, Chinese Academy of Sciences) for supporting the chemical library. We thank our Sustech colleagues Dr. Hua Li, Dr. Lin Lin, and Ms. Suying Gao for mass spectrometry analyses, Dr. Xing Wen, Ms. Qiuhua Yang, and Dr. Yuping Qiu for assistance in protein purification, Ms. Qian Gao for the supporting of the RNA-seq analysis, and all members in Guo lab for stimulating discussion and suggestions. We thank the staffs of the BL17B1/BL18U1/BL19U1/BL19U2/BL01B beamlines of National Facility for Protein Science in Shanghai (NFPS) at Shanghai Synchrotron Radiation Facility for assistance during data collection. This work was supported by the National Natural Science Foundation of China (Grants No. 32230008 and 31911540070 to H.G. and Grant No. 21907049 to K.J.), the National Key Research and Development Program of China (Grant 2019YFA0903904 to H.G.), a JSPS Grant-in-Aid for Scientific Research (Grant 18H05266) to T.A., the Key Laboratory of Molecular Design for Plant Cell Factory of Guangdong Higher Education Institutes (2019KSYS006 to H.G.), the Guangdong Innovative and Entrepreneurial Research Team Program (Grant No. 2016ZT06S172) to K.J., the Shenzhen Science and Technology Program (Grant No. KYTDPT20181011104005 to K.J. and Grant No. KQTD20190929173906742 to H.G.), and the China Postdoctoral Science Fund Project (Grant No. 2020M672406 to Y.X.).

Author affiliations: [a]Institute of Plant and Food Science, Department of Biology, School of Life Sciences, Southern University of Science and Technology, Shenzhen, Guangdong 518055, China; [b]Key Laboratory of Molecular Design for Plant Cell Factory of Guangdong Higher Education Institutes, School of Life Sciences, Southern University of Science and Technology, Shenzhen, Guangdong 518055, China; [c]Institute for Advanced Studies, Wuhan University, Wuhan 430072, P.R. China; [d]Graduate School of Agricultural and Life Sciences, The University of Tokyo, Tokyo 1138657, Japan; [e]Section of Cell and Developmental Biology, University of California San Diego, La Jolla, CA 92093; and [f]Jiangsu Key Laboratory for Biodiversity and Biotechnology, College of Life Sciences, Nanjing Normal University, Nanjing 210023, China

Author contributions: Y.X., Y.Z., H.H., H.G., and K.J. designed research; Y.X., Y.Z., N.W., M.L., T.O., R.G., I.T., Z.Y., Y.A., L.Z., Y.Y., Y.J.Z., H.B., Y.W., Z.Z., A.C.H., and K.J. performed research; Y.D.Z. and T.A. contributed new reagents/analytic tools; Y.X. and H.H. analyzed data; and Y.X., N.W., H.H., H.G., and K.J. wrote the paper.

1. S. Roychoudhry, S. Kepinski, Auxin in root development. *Cold Spring Harb. Perspect. Biol.* **14**, a039933 (2022).
2. P. Overvoorde, H. Fukaki, T. Beeckman, Auxin control of root development. *Cold Spring Harb. Perspect. Biol.* **2**, a001537 (2010).
3. K. Ljung, Auxin metabolism and homeostasis during plant development. *Development* **140**, 943–950 (2013).
4. A. N. Stepanova, J. M. Alonso, Auxin catabolism unplugged: Role of IAA oxidation in auxin homeostasis. *Proc. Natl. Acad. Sci. U.S.A.* **113**, 10742–10744 (2016).
5. Z. Zhao *et al.*, A role for a dioxygenase in auxin metabolism and reproductive development in rice. *Dev. Cell* **27**, 113–122 (2013).
6. S. Porco *et al.*, Dioxygenase-encoding *AtDAO1* gene controls IAA oxidation and homeostasis in *Arabidopsis*. *Proc. Natl. Acad. Sci. U.S.A.* **113**, 11016–11021 (2016).
7. J. Zhang *et al.*, DAO1 catalyzes temporal and tissue-specific oxidative inactivation of auxin in *Arabidopsis thaliana*. *Proc. Natl. Acad. Sci. U.S.A.* **113**, 11010–11015 (2016).
8. P. E. Staswick, I. Tiryaki, M. L. Rowe, Jasmonate response locus *JAR1* and several related Arabidopsis genes encode enzymes of the firefly luciferase superfamily that show activity on jasmonic, salicylic, and indole-3-acetic acids in an assay for adenylation. *Plant Cell* **14**, 1405–1415 (2002).
9. P. E. Staswick *et al.*, Characterization of an Arabidopsis enzyme family that conjugates amino acids to indole-3-acetic acid. *Plant Cell* **17**, 616–627 (2005).
10. R. A. Okrent, M. C. Wildermuth, Evolutionary history of the GH3 family of acyl adenylases in rosids. *Plant Mol. Biol.* **76**, 489–505 (2011).
11. K. I. Hayashi *et al.*, The main oxidative inactivation pathway of the plant hormone auxin. *Nat. Commun.* **12**, 6752 (2021).
12. C. S. Westfall *et al.*, *Arabidopsis thaliana* GH3.5 acyl acid amido synthetase mediates metabolic crosstalk in auxin and salicylic acid homeostasis. *Proc. Natl. Acad. Sci. U.S.A.* **113**, 13917–13922 (2016).
13. P. E. Staswick, I. Tiryaki, The oxylipin signal jasmonic acid is activates by an enzyme that conjucates it to isoleucine in Arabidopsis. *Plant Cell* **16**, 2117–2127 (2004).
14. C. K. Holland *et al.*, Brassicaceae-specific Gretchen Hagen 3 acyl acid amido synthetases conjugate amino acids to chorismate, a precursor of aromatic amino acids and salicylic acid. *J. Biol. Chem.* **294**, 16855–16864 (2019).
15. D. Rekhter *et al.*, Isochorismate-derived biosynthesis of the plant stress hormone salicylic acid. *Science.* **365**, 498–502 (2019).
16. H. E. Blackwell, Y. Zhao, Chemical genetic approaches to plant biology. *Plant Physiol.* **133**, 448–455 (2003).
17. G. R. Hicks, N. V. Raikhel, Small molecules present large opportunities in plant biology. *Annu. Rev. Plant Biol.* **63**, 261–282 (2012).
18. K. Jiang, T. Asami, Chemical regulators of plant hormones and their applications in basic research and agriculture. *Biosci. Biotechnol. Biochem.* **8451**, 1–36 (2018).
19. K. Fukui, K. I. Hayashi, Manipulation and sensing of auxin metabolism, transport and signaling. *Plant Cell Physiol.* **59**, 1500–1510 (2018).
20. C. Böttcher *et al.*, A novel tool for studying auxin-metabolism: The inhibition of grapevine indole-3-acetic acid-amido synthetases by a reaction intermediate analogue. *PLoS One* **7**, 1–8 (2012).
21. K. Fukui *et al.*, Chemical inhibition of the auxin inactivation pathway uncovers the roles of metabolic turnover in auxin homeostasis. *Proc. Natl. Acad. Sci. U.S.A.* **119**, e2206869119 (2022).
22. G. Hagen, T. J. Guilfoyle, Rapid induction of selective transcription by auxins. *Mol. Cell. Biol.* **5**, 1197–1203 (1985).
23. C. Timpte, A. K. Wilson, M. Estelle, The *axr2-1* mutation of *Arabidopsis thaliana* is a gain-of-function mutation that disrupts an early step in auxin response. *Genetics* **138**, 1239–1249 (1994).
24. P. Nagpal *et al.*, *AXR2* encodes a member of the Aux/IAA protein family. *Plant Physiol.* **123**, 563–573 (2000).
25. W. He *et al.*, A small-molecule screen identifies L-Kynurenine as a competitive inhibitor of TAA1/TAR activity in ethylene-directed auxin biosynthesis and root growth in Arabidopsis. *Plant Cell* **23**, 3944–3960 (2011).
26. Y. Kakei *et al.*, Small-molecule auxin inhibitors that target YUCCA are powerful tools for studying auxin function. *Plant J.* **84**, 827–837 (2015).
27. E. J. Chapman, M. Estelle, Mechanism of auxin-regulated gene expression in plants. *Annu. Rev. Genet.* **43**, 265–285 (2009).
28. I. A. Paponov *et al.*, Comprehensive transcriptome analysis of auxin responses in Arabidopsis. *Mol. Plant* **1**, 321–337 (2008).
29. D. R. Lewis *et al.*, A kinetic analysis of the auxin transcriptome reveals cell wall remodeling proteins that modulate lateral root development in Arabidopsis. *Plant Cell* **25**, 3329–3346 (2013).
30. R. Mackelprang, R. A. Okrent, M. C. Wildermuth, Preference of Arabidopsis thaliana GH3.5 acyl amido synthetase for growth versus defense hormone acyl substrates is dictated by concentration of amino acid substrate aspartate. *Phytochemistry* **143**, 19–28 (2017).
31. C. S. Westfall *et al.*, Structural basis for prereceptor modulation of plant hormones by GH3 proteins. *Science* **336**, 1708–1711 (2012).
32. Q. Chen, C. S. Westfall, L. M. Hicks, S. Wang, J. M. Jez, Kinetic basis for the conjugation of auxin by a GH3 family indole-acetic acid-amido synthetase. *J. Biol. Chem.* **285**, 29780–29786 (2010).
33. R. A. Okrent, M. D. Brooks, M. C. Wildermuth, Arabidopsis GH3.12 (PBS3) conjugates amino acids to 4-substituted benzoates and is inhibited by salicylate. *J. Biol. Chem.* **284**, 9742–9754 (2009).
34. A. Round *et al.*, Determination of the GH3.12 protein conformation through HPLC-integrated SAXS measurements combined with X-ray crystallography. *Acta Cryst. D* **69**, 2072–2080 (2013).
35. A. M. Sherp, S. G. Lee, E. Schraft, J. M. Jez, Modification of auxinic phenoxyalkanoic acid herbicides by the acyl acid amido synthetase GH3.15 from Arabidopsis. *J. Biol. Chem.* **293**, 17731–17738 (2018).
36. A. M. Sherp, C. S. Westfall, S. Alvarez, J. M. Jez, *Arabidopsis thaliana* GH3.15 acyl acid amido synthetase has a highly specific substrate preference for the auxin precursor indole-3-butyric acid. *J. Biol. Chem.* **293**, 4277–4288 (2018).
37. C.-Y. Chen, S.-S. Ho, T.-Y. Kuo, H.-L. Hsieh, Y.-S. Cheng, Structural basis of jasmonate-amido synthetase FIN219 in complex with glutathione S-transferase FIP1 during the JA signal regulation. *Proc. Natl. Acad. Sci. U. S. A.* **114**, E1815–E1824 (2017).
38. J. Jumper *et al.*, Highly accurate protein structure prediction with AlphaFold. *Nature* **596**, 583–589 (2021).
39. B. Steffens, A. Rasmussen, The physiology of adventitious roots. *Plant Physiol.* **170**, 603–617 (2016).
40. Q. Liu *et al.*, OsIAGT1 is a glucosyltransferase gene involved in the glucose conjugation of auxins in rice. *Rice* **12**, 92 (2019).
41. R. Guo *et al.*, Local conjugation of auxin by the GH3 amido synthetases is required for normal development of roots and flowers in Arabidopsis. *Biochem. Biophys. Res. Commun.* **589**, 16–22 (2022).
42. M. Nakazawa *et al.*, *DFL1*, an auxin-responsive GH3 gene homologue, negatively regulates shoot cell elongation and lateral root formation, and positively regulates the light response of hypocotyl length. *Plant J.* **25**, 213–221 (2001).
43. T. Takase *et al.*, *ydk1-D*, an auxin-responsive GH3 mutant that is involved in hypocotyl and root elongation. *Plant J.* **37**, 471–483 (2004).
44. J. E. Park *et al.*, GH3-mediated auxin homeostasis links growth regulation with stress adaptation response in Arabidopsis. *J. Biol. Chem.* **282**, 10036–10046 (2007).
45. P. Sukumar, G. S. Maloney, G. K. Muday, Localized induction of the ATP-binding cassette B19 auxin transporter enhances adventitious root formation in Arabidopsis. *Plant Physiol.* **162**, 1392–1405 (2013).
46. Z. Zheng *et al.*, Local auxin metabolism regulates environment-induced hypocotyl elongation. *Nat. Plants* **2**, 1–9 (2016).
47. R. Di Mambro *et al.*, The lateral root cap acts as an auxin sink that controls meristem size. *Curr. Biol.* **29**, 1199–1205.e4 (2019).